Prototype Repository

Estimation of the buffer homogenisation

Mattias Åkesson
Svensk Kärnbränslehantering AB

Abstract

The Prototype Repository is a full-scale field experiment in crystalline rock at a depth of 450 m in the Äspö Hard Rock Laboratory. The experiment consists of six deposition holes with copper canisters, with electrical heaters, and with MX-80 bentonite buffer. The buffer was installed in 2001- 2003 as compacted blocks and by filling the outer slot between the blocks and the rock wall with bentonite pellets. The inner section of the experiment will be retrieved beginning in 2023, and different pre-modelling activities have been part of the planning of this operation.

The aim of this work has been to estimate the buffer homogenization in the Prototype Repository. Two types of models have been analysed: i) 1D axisymmetric models with either fast or slow hydration, and with or without a thermal gradient. These models address the issue of the rate of hydration and how this influences the extent of remaining heterogeneity at full saturation; and ii) 2D models with a circular geometry. These are used for analysing the issue of horizontal movements of the canister caused by the uneven wetting of the buffer. The modelling was performed with COMSOL Multiphysics, and for describing the hydromechanical processes in the bentonite, the Hysteresis Based Material (HBM) model was used.

Sammanfattning

Prototypförvaret är ett fullskaligt fältförsök i kristallint berg på ett djup av 450 meter i Äspö-laboratoriet (Äspö HRL). Försöket har bestått av sex deponeringshål med kopparkapslar, med elektriska värmare, och med en buffert av MX-80 bentonit. Bufferten installerades under 2001 - 2003 som kompakterade block och genom att fylla den yttre spalten mellan block och bergvägg med bentonit-pellets. Den inre sektionen av försöket kommer att återtas med början av 2023, och olika förmodelleringsaktiviteter har utförts under planeringen av denna operation.

Målet med detta arbete har varit att göra en uppskattning av bufferthomogeniseringens omfattning i Prototypförvaret. Två typer av modeller har analyserats: i) 1D axisymmetriska modeller med snabb eller långsam bevätning, samt med eller utan en termisk gradient. Dessa modeller tar i tu med frågeställningen om bevätningshastigheten och hur denna påverkar den kvarvarande heterogenitet vid full vattenmättnad; och ii) 2D modeller med en cirkulär geometri. Dessa används för att analysera frågeställningen om horisontella kapselrörelser som orsakas av en ojämn bevätning av bufferten. Modelleringen utfördes med COMSOL Multiphysics, och för att beskriva de hydromekaniska processerna i bentoniten användes den Hysteresbaserade materialmodellen (HBM).

Content

1   Background

The Prototype Repository is a full-scale field experiment in crystalline rock at a depth of 450 m in the Äspö Hard Rock Laboratory (Äspö HRL). The experiment aims to simulate conditions largely relevant to the Swedish/Finnish KBS-3V disposal concept for spent nuclear fuel. The experiment consists of six deposition holes with copper canisters (with electrical heaters) and with bentonite (MX-80) buffer. The buffer was installed as compacted blocks and by filling the outer slot between the blocks and the rock wall with bentonite pellets. The test-tunnel was divided into two separate sections and backfilled and finally sealed by two reinforced concrete dome plugs. The inner section, with four deposition holes, was installed in 2001, whereas the outer section, with two deposition holes, was installed in 2003 and subsequently retrieved in 2010/2011. The inner section will be retrieved beginning in 2023, and different pre-modelling activities have been part of the planning of this operation. The aim of this work has been to estimate the buffer homogenisation in the Prototype Repository.

2 Dismantling data from the outer section

An extensive and detailed analysis regarding the water content and the density of the buffer was performed during the course of the dismantling of the outer section (Johannesson 2014). These measurements demonstrated that the buffer had homogenised to a large extent, but also that a remaining heterogeneity could be noted between the inner and outer parts of the buffer. Differences between the dry density in different directions could also be observed (Figure 2-1 to Figure 2-3). Moreover, the distribution of the water content and the dry density in some sections in both deposition holes (Dh5 and Dh6) showed that the wetting and the swelling in one direction was much larger than in the opposite direction, and this indicates that the buffer and the canister was displaced in horizontal direction.

An alternative explanation for this could possibly be that the canisters and the buffer blocks were initially installed slightly shifted from the centre of the deposition holes, and that the side with a relatively wide pellet-filled slot would promote preferential wetting in that direction. Such a situation could possibly yield dismantling data in which the water contents and the dry densities are correlated. A third, more theoretical, explanation could possibly be that the horizonal position of the canister is fixed, and that bentonite largely redistributes through tangential swelling. However, a horizontal displacement of the canister appears to be supported by the sensors data in Dh6 (see Chapter 6).

A one-sided swelling may be correlated with the mapped fractures in the case of Dh5, but this does not seem to be a likely explanation for Dh6. Instead, the potential formation of a conducting channels in the pellets-filled slot has been addressed in the saturation modelling task. It has also motivated an approach with free access of water, in some cases with a fairly high water pressures, at the boundary in some of the models presented in this work.

It can also be noted that the displacement pattern was more pronounced in the upper part of the buffer. In Dh6 the lowest dry density in each block was nevertheless found in the same direction along the entire depth of the deposition hole (Figure 2-2). In contrast, in Dh5 the directions with the lowest dry density was different in the upper and lower parts of Dh5, and this could be interpreted as the canister was slightly tilted in this deposition hole.

Apart from the horizontal movements, the buffer in both deposition holes was largely influenced by the upward swelling. The interface between the upper buffer block and the backfill had moved 0.18 and 0.15 m upwards in Dh6 and Dh5, respectively (Svemar et al. 2016). This is also reflected by a general increase in water content and decrease in dry density in the upper part of the buffer, especially the uppermost cylinders (Figure 2-1 to Figure 2-3).

The dismantling data can potentially be used in at least two ways for analysing the buffer homogenisation: i) by comparing model results with experimental data, and ii) by evaluating the remaining level of heterogeneity from the dismantling data. The first approach is complicated by the fact that the data from rings appear in most cases to be influenced by horizontal displacement making it difficult to make comparison with axisymmetric models. The rings that appear to be least affected by displacements are R1 Dh6, and R2/3 Dh5, whereas the most affected rings appear to be R8 Dh6 and R6/7 Dh5. The second approach could for instance be followed by evaluating the difference in dry density across the interface between the block and the pellets. The data from the so-called end-sectors may potentially reveal this information, but it appears to be difficult to identify this interface in a systematic manner.

Another observation that can be made for the dismantling data is that the driest parts of rings in Dh5 and Dh6 exhibit water contents at least 2 % higher than the initial value (e.g. R8 Dh6 and R7 Dh5) and this may be interpreted as a "matrix flow" which hydrates the buffer with a restricted rate, and this has motivated the use of hydraulic boundary conditions with low flow rates in some of the models presented in this work.
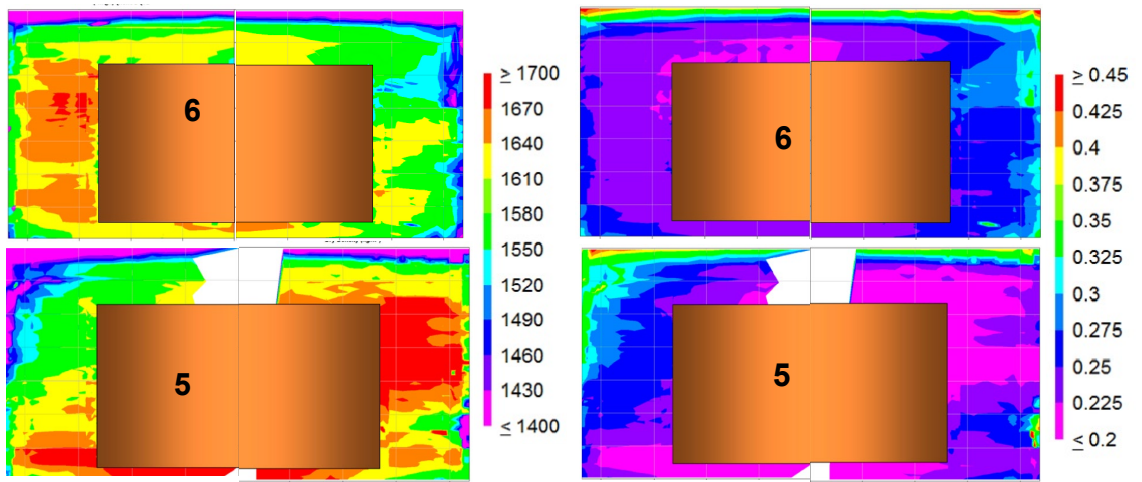
Figure 2-1. Contour plots of measured dry density (kg/m³, left) and water content (-, right); composite plot for two opposite directions in deposition hole 6 (upper) and 5 (lower). Original plots presented by Johannesson (2014).
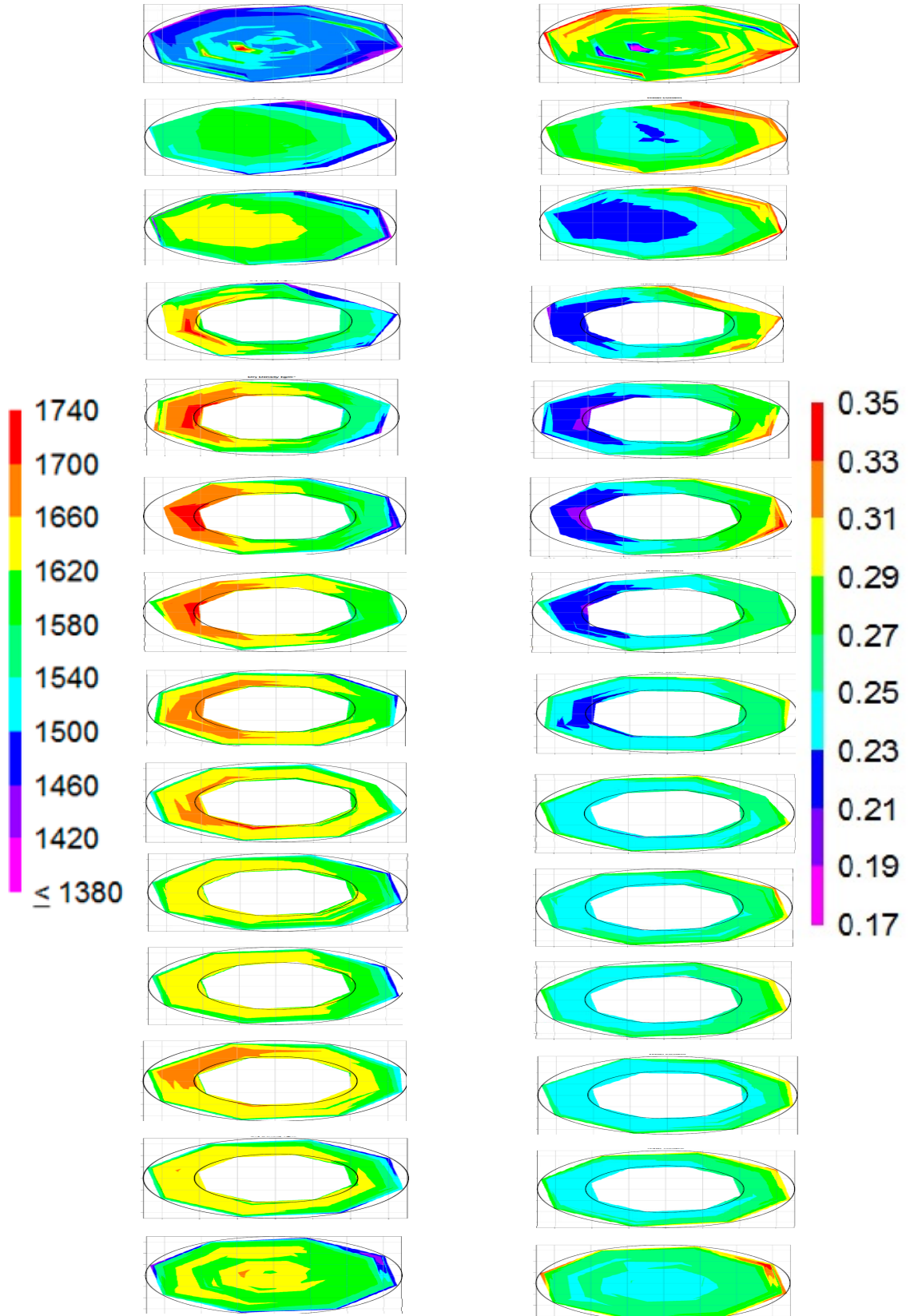
Figure 2-2. Contour plots of measured dry density (kg/m³, left) and water content (-, right); composite plot for all blocks in deposition hole 6 presented by Johannesson (2014). It should be observed that the colours of the uppermost block (C4) corresponds to dry density values which were slightly lower than those indicated by the scale. Correspondingly, the water contents were slightly higher.

5

Figure 2-3. Contour plots of measured dry density (kg/m³, left) and water content (-,right); composite plot for all blocks in deposition hole 5 presented by Johannesson (2014). It should be observed that the colours of the uppermost block (C4) corresponds to dry density values which were slightly lower than those indicated by the scale. Correspondingly, the water contents were slightly higher.
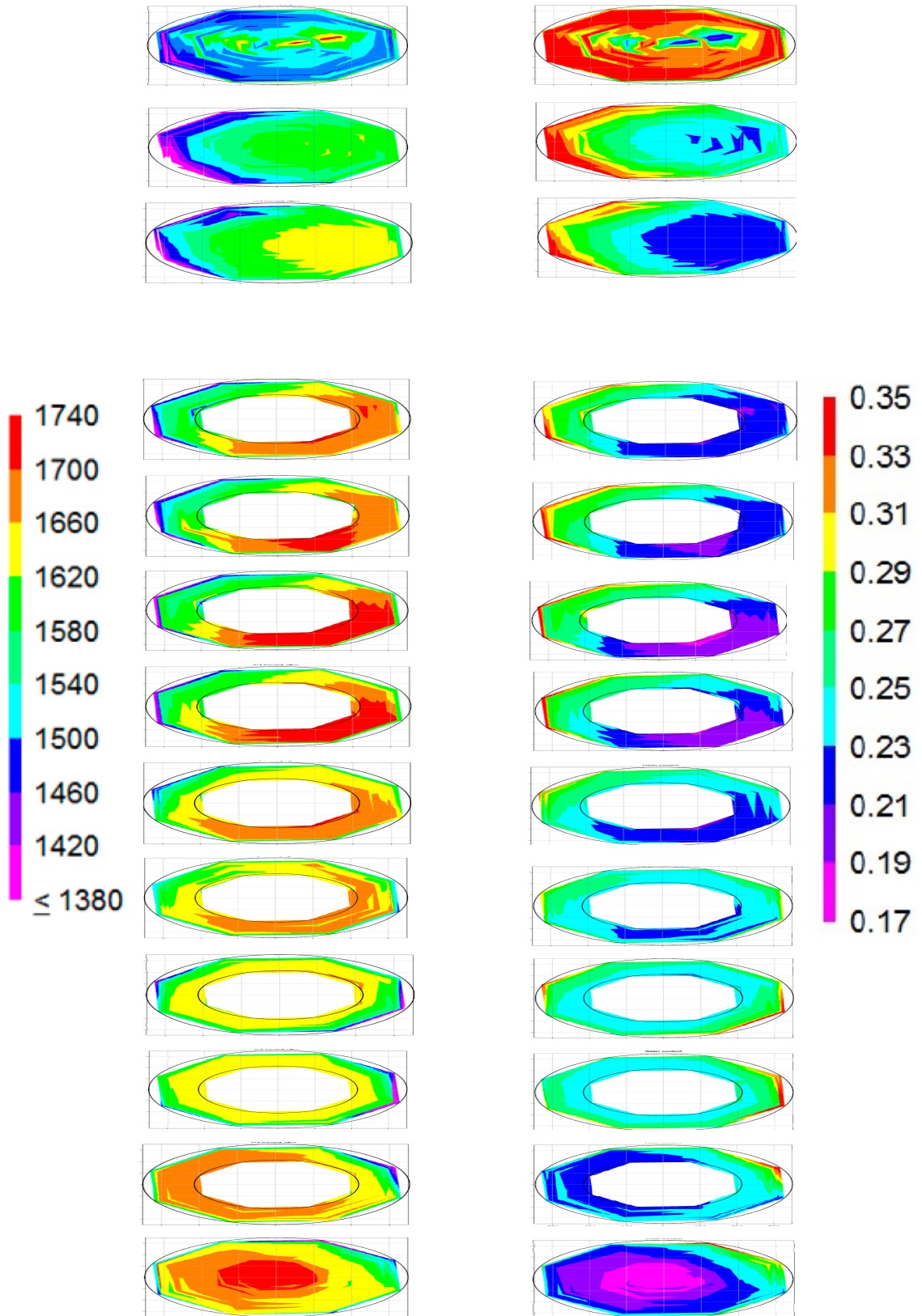
3 Model description

3.1 General strategy

The focus of this work has been on the buffer sections around the canister. The main motive for this was that the buffer rings were less influenced by upward swelling than the cylinders, especially the upper cylinders.

Moreover, the models are generic in the sense that both the hydraulic and the thermal boundary conditions are simplified. The reason for this was that it is not possible to make predictions of any specific part of the buffer, since "the uncertainties in the measured inflows to the deposition holes were too large to make a precise calibration of the rock surrounding the deposition holes" as was noted for the TH modelling of the outer section (Svemar et al. 2016), and since some of the heaters in the canister have failed during the test period.

Two types of models have been analysed: i) 1D axisymmetric models with either fast or slow hydration, and with or without a thermal gradient. These models address the issue of the rate of hydration and how this influences the extent of remaining heterogeneity at full saturation; and ii) 2D models with a circular geometry. These are used for analysing the issue of horizontal movements of the canister caused by the uneven wetting of the buffer.

The modelling was performed with COMSOL Multiphysics, and for describing the hydromechanical processes in the bentonite, the Hysteresis Based Material (HBM) model was used (Appendix A). This model was first defined during the course of the homogenisation project (Dueck et al. 2019) and the related modelling task (Börgesson et al. 2020). The definition and the implementation of this has been further developed within the framework of the BEACON project.

3.2 Geometry. Initial conditions. Boundary conditions. Model cases

The 1D geometry is shown in Figure 3-1. The dimensions were essentially the same as for the current reference design, but the width of the pellets-filled slot was 60 mm instead of 50 mm. The initial dry density of the block and pellets were 1798 and 1053 kg/m^3, respectively, corresponding to the void ratios 0.546 and 1.64. Together with an inner slot of 10 mm, this corresponds to a homogenized dry density of 1608 kg/m^3, which is the value stated for the ring section in Dh4 in the installation report (Börgesson et al. 2002). The initial water content was 17 and 13 % for the blocks and pellets respectively. The geometry was discretized in a mesh with a row of 76 quadrilateral elements.

Roller boundaries were used on all sides except for the inner, for which a spring boundary was used to represent the closure of the inner slot. A special interface material (0.5 mm thick) between the blocks and the pellets was required in order to handle the difference in the initial suction values in these two materials (see Charlier et al. 2021, section 3.3.2, for details). Thermal and hydraulic boundary conditions were applied on the inner side (no water flow) and on the outer side of the buffer (see Table 3-1). Four model cases were analysed. Two of these were isothermal cases (indicated with "IT" in the name) with a constant temperature of 15 °C (representing the initial conditions in the Prototype tunnel), while the other two were thermal cases (with "T" in the name) with thermal boundary conditions of 75 and 55 °C on the inner and outer boundary, respectively (representing a fairly typical temperature range across the buffer, see e.g. Ring 5 in Dh5). These boundary conditions were ramped from an initial level of 15 °C during the first 90 days. Moreover, two of the model cases (denoted "Fast") had free access of water with a constant liquid pressure at the outer boundary, whereas the remaining two cases (denoted "Slow") had restricted access with a constant flow rate at the outer boundary. An atmospheric boundary pressure (0.1 MPa absolute) was used for the isothermal model cases, both as a pressure condition in the fast case and as a maximum pressure in the slow case. An atmospheric pressure would however yield a quite slow wetting in the thermal case with a pressure boundary and the boundary pressure were therefore set to 1.1 MPa absolute for the two thermal cases.

The 2D geometry is shown in Figure 3-2. This problem was found to be much more numerically demanding than the 1D geometry, and therefore some simplifications were made: i) the pellets had the same initial water content as the blocks (i.e. 17 %), ii) the inner slot was omitted by assuming that the block has swelled and homogenized into this from the start, iii) only isothermal conditions at 20 °C were considered, and iv) the dimensions and initial dry densities and water content followed the current reference design of KBS-3, with the void ratio for pellets 1.78, and for blocks 0.571. Assuming that the block had swelled and homogenized into the 10 mm inner slot, a void ratio of 0.613 was used for this component. Roller boundaries were used on all sides except for the inner which was free to move. In should be noted that the block was attached to the canister material. Two different hydraulic boundary conditions were applied on the outside of the geometry. The 1st condition was a constant liquid (gage) pressure of 1 MPa along an arc which spans 1/6 of the circumference. The 2nd condition was a constant flow rate which corresponded to a saturation time of approximately 20 years. In one of the model cases (2D_dry), only the 1st condition was used, whereas in the second case (2D_wet) both conditions were used (see Table 3-1). The geometry was discretized in a mesh with 8 x 57 = 456 quadrilateral elements. The radial width of the pellets-filled slot was discretised in one element, whereas the width of the bentonite block was divided in 6 elements.

The constitutive relations and the parameter values used for describing the bentonite properties are presented in Appendix A. The canister included in the 2D-models was described as a linear elastic material with very high stiffness ($E = 10^{13}$ Pa; $\nu = 0.2$) and without any representation thermo-hydraulic processes. Finally, it should be noted that it was difficult to reach convergence for the 2D models, and this was the main reason for using the crude mesh in these cases. No attempt to investigate the influence of the mesh size on the solution was made.
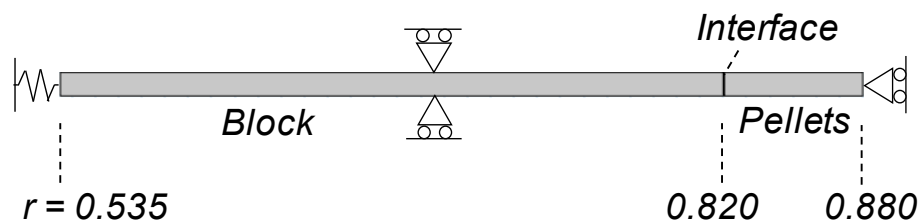

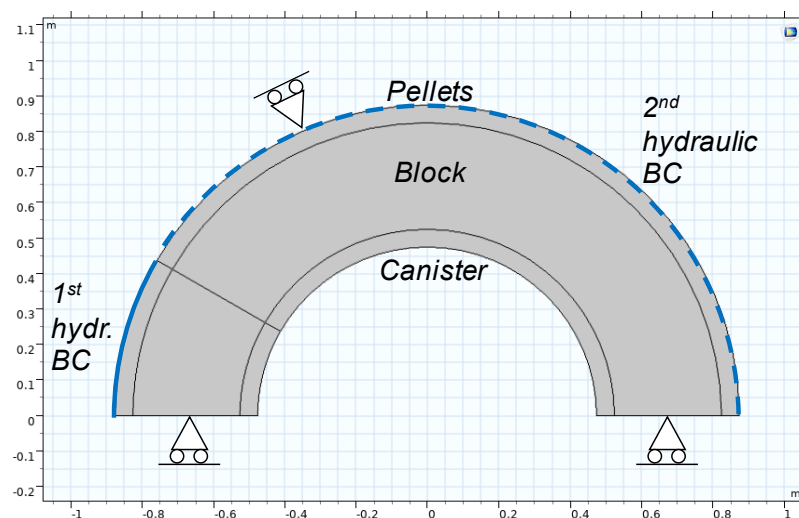*Figure 3-1. 1D geometry and mechanical boundary conditions.*

Figure 3-2. 2D geometry and boundary conditions. Inner and outer block radius 0.525 and 0.825 mm, respectively. Rock wall radius 0.875 mm).

Table 3-1. Model cases and different boundary conditions.

Model	Hydraulic BC[1] [2]		Thermal BC (°C)
	Constant pressure (MPa)	Constant flow rate[3] (kg/m2,s)	
Slow_IT	-	7e-8, (max 0.1 MPa)	15
Fast_IT	0.1	-	15
Slow_T	-	9e-8 (max 1.1 MPa)	75/55
Fast_T	1.1	-	75/55
2D_dry	1.1	-	20
2D_wet	1.1	1e-7 (max 1.1 MPa)	20

1) All hydraulic boundary conditions were actually flow boundaries, for which the prescribe flux decreased to zero when the pressure reach the prescribed value.
2) Pressures given as absolute values
3) First value shows the flow rate, whereas the value in parenthesis shows the maximum pressure.

4 Results 1D model

The overall behaviour of the different model cases model is illustrated in Figure 4-1 and Figure 4-2. The evolution of RH and radial stresses displays increasing trends, except for the early evolution of RH in the inner part of the models with a thermal gradient. These trends show that the models with free access of water was fully water saturated and equilibrated after approximately 8-12 years,
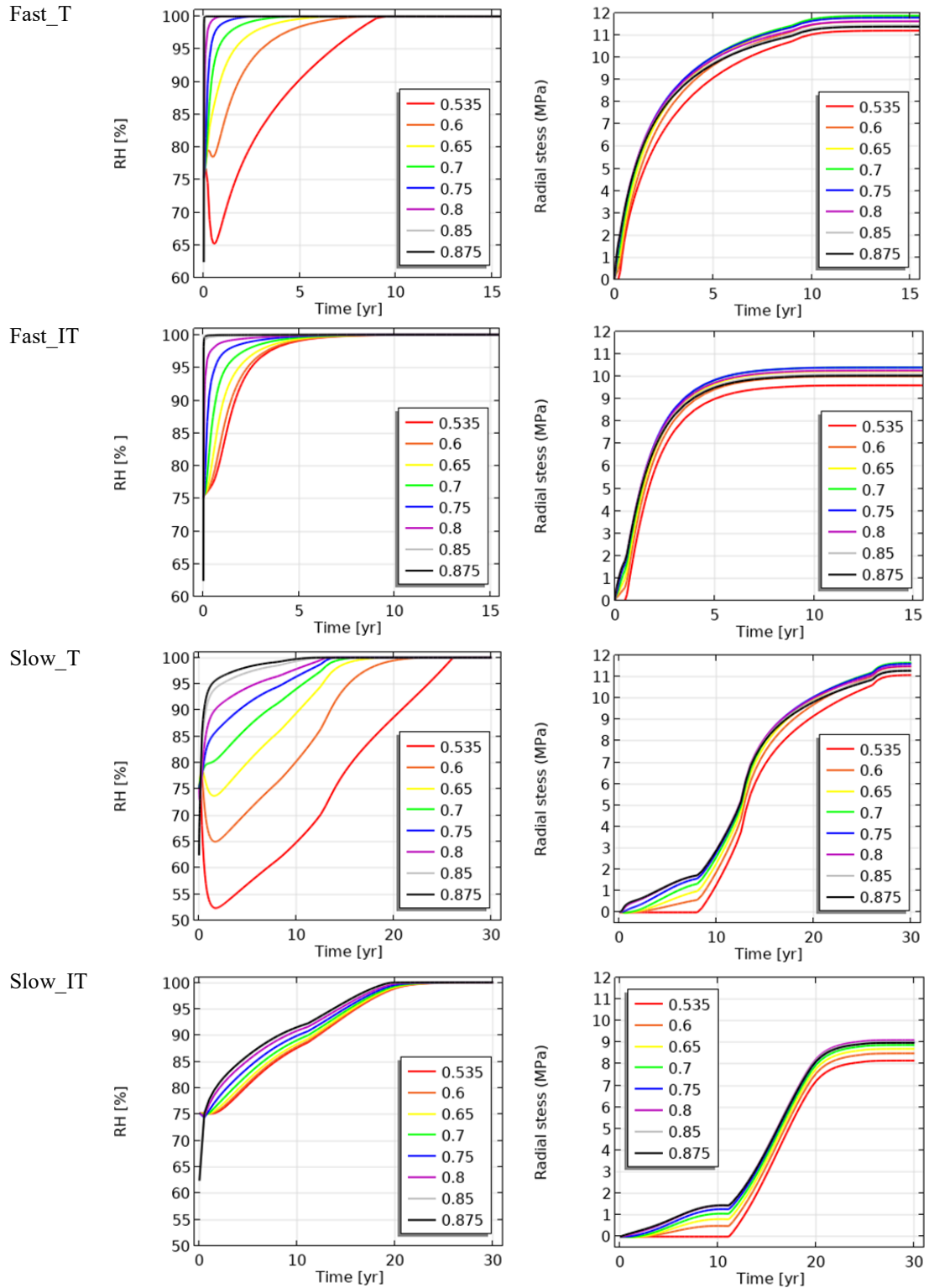

Figure 4-1. Evolution of RH (left) and radial stress (right) at eight positions in the different 1D model cases.

whereas the models with restricted water uptake reached this state after approximately 26-28 years. It can be noted that the overall stress level is in general agreement with the measured total pressures shown in Figure 4-4, which shows data from Ring 1 and Ring 2 in Dh6. It should be noted that the corresponding evolution of total pressure in Ring 6 in Dh6 displayed a slower build-up and ended up at a lower pressure level (~ 7.5–9.0 MPa; see Goudarzi 2014) which could possibly reflect an influence of upward swelling, or that the wetting was slower, at this level in the deposition hole.
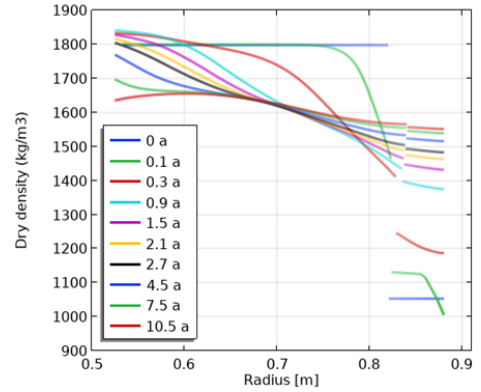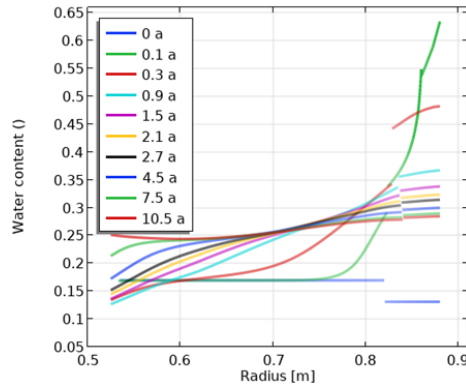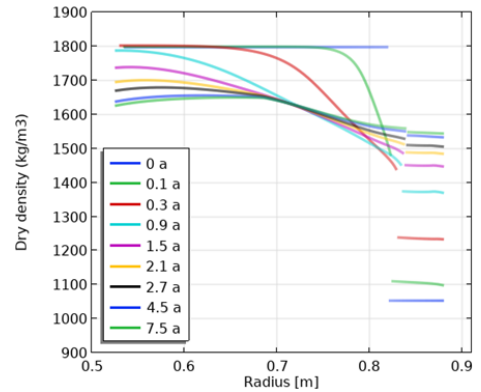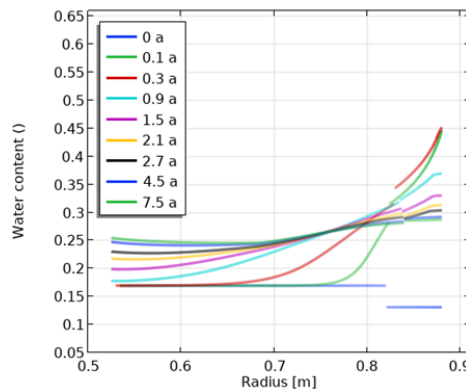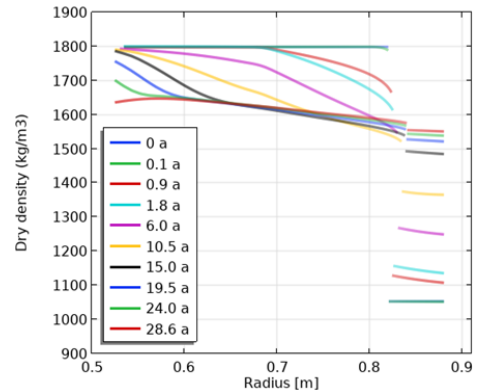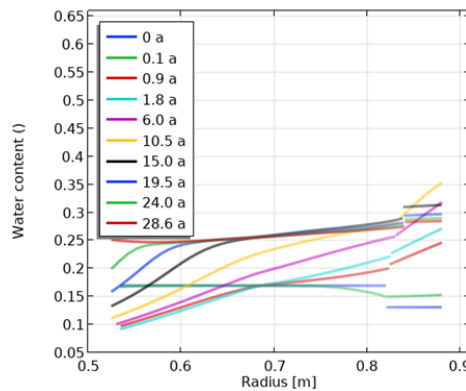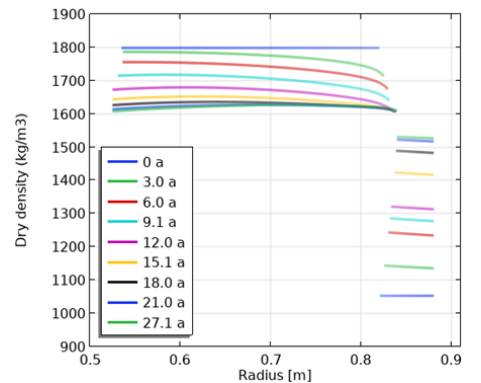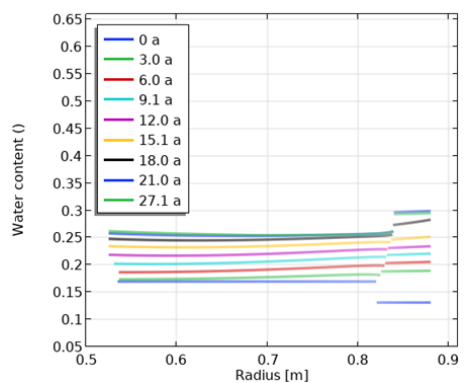

Figure 4-2. Distributions of water content (left) and dry density (right) for different times in the 1D model cases.

Radial distributions of water content and dry density at different times (see Figure 4-2) illustrate the water uptake and the homogenisation of the buffer. The initial dehydration in the inner part of the models with thermal gradient can be noted. The final state along the geometry is shown in terms of mean effective stress versus the dry density, and of the von Mises stress versus mean effective stress in Figure 4-3. This illustrates that the used material model inherently yields results which are consistent with experimental data regarding the swelling pressure and the shear strength. A compilation of the final dry density distributions for the different modelling cases is shown in Figure 4-5. In can be noted that the overall density level is in general agreement with the dismantling data (see lower panels). Still, the buffer in Dh5 and Dh 6 displayed a significant heterogeneity at the time of the dismantling (see Figure 2-2 and 2-3). A dry density distribution for Ring 6 in Dh6 for instance is nevertheless quite similar to the distribution in Figure 4-5, although the dry density in the innermost part was slightly higher (see Johannesson 2014).

The model results show that the largest heterogeneity in terms of the difference in dry density across the block-pellets interface, and the lowest dry density in the pellets filling, is found for the case with a slow hydration and without a thermal gradient. Cases with either a rapid hydration, and/or with a thermal gradient will result in more homogenous end-states. This result is a consequence of the HBM model and is caused by the fact that the outer part of the blocks in all the model cases, except the slow isothermal cases, undergoes a swelling/compression cycle which leads to a relatively continuous distribution in the final state. In contrast, the block in the slow isothermal case undergoes "pure" swelling which leads to a discreet distribution in the final state (see dry density profiles in Figure 4-2). This in turn leads to a denser block and therefore, due to the fixed volume of the system, a relatively low dry density of the compressed pellets.
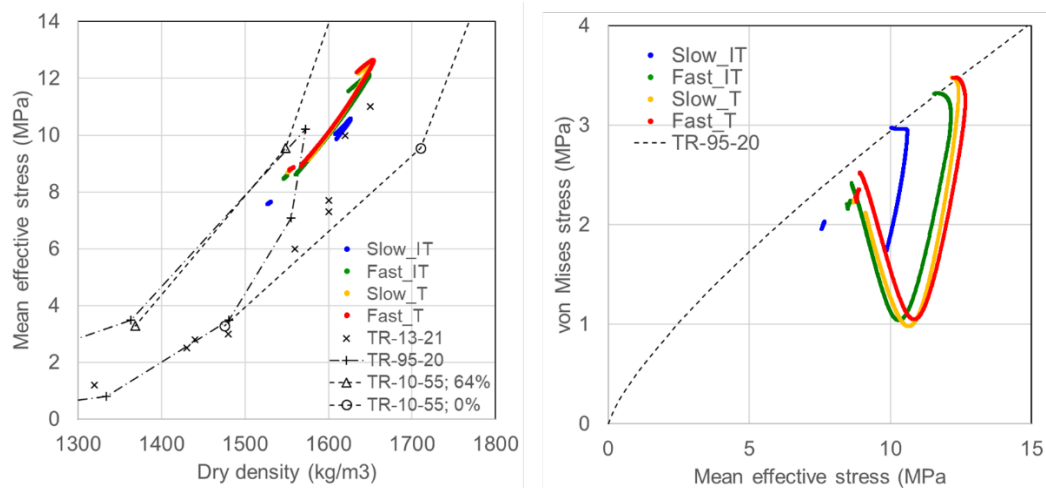

Figure 4-3. Final state regarding mean effective stress vs dry density (left), and von Mises stress versus mean effective stress (right) for different model cases (coloured circles). Experimental data marked for comparison: TR-13-21 is swelling pressure data from Olsson et al. (2013); TR-95-20 in the left graph is axial stresses from a saturated oedometer test, from Börgesson et al. (1995), while the line in the right graph is an empirical relationship between the maximum von Mises stress versus the mean effective stress adopted from different triaxial compression tests; TR-10-55 is water retention data for samples with different initial water content (0 and 64 %) at free swelling conditions from Dueck and Nilsson (2010) for which the relative humidity was converted to a pressure (see Dueck at al. 2019) and the water content converted to a dry density at saturated conditions.
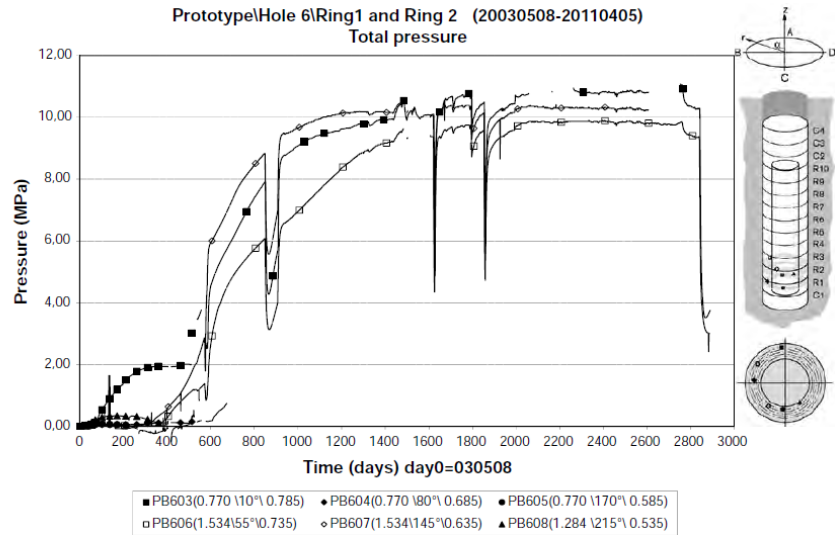
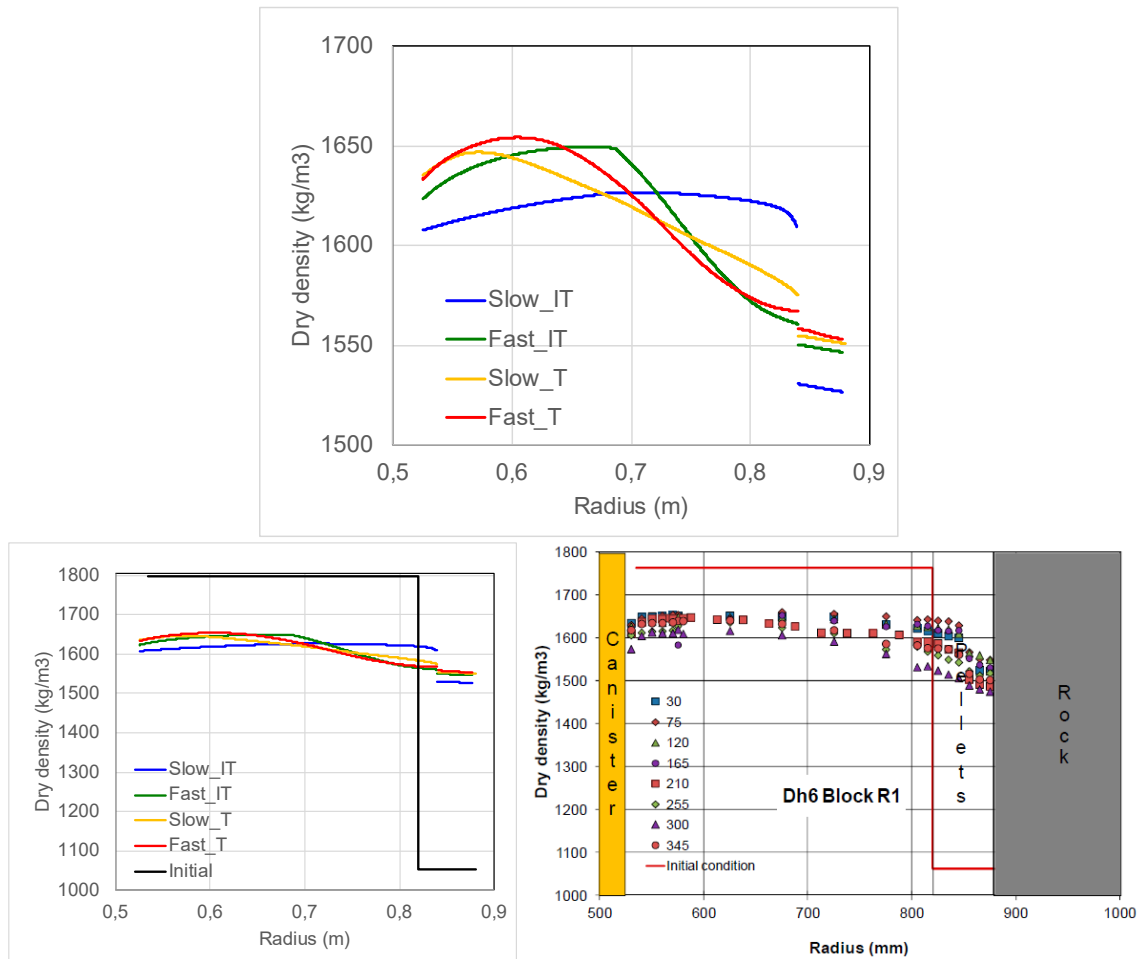**Figure 4-4. Measured total pressures in R1 and R2 in Dh6.**

Figure 4-5. Final dry density distribution – all cases (top & left). Dismantling data from R1 Dh6 (right).

14

5   Results 2D model

Dry density distributions after approximately 8 and 21 years, and the evolution of the horizontal displacement of the canister, is shown for dry and the wet model cases in Figure 5-1 and 5-2, respectively. It should be noted that the 2D plots with the density distributions do not take displacements into account, which means that the pellets-filled slot is wider than it would if the displacements were considered.

The times chosen correspond to times of dismantling of the outer and inner section. The results for the dry model for 8 years is quite heterogenous and resemble the dismantling data for Ring 6 and 7 in Dh5 shown in Figure 2-3, and to a lesser extent the more homogenous conditions in Dh6 (Figure 2-3). In contrast, the wet model for the same time displays a more homogenous density distribution and is thereby more similar to the experimental data in Dh6.

The displacement plots show that the time to saturate (and equilibrate) the dry case is very long (over 300 years), whereas the wet case is approximately 10 times faster. The maximum displacement is also reached faster than in the dry case, but with a significantly lower value (11-12 mm instead of 18-19 mm). These results can be compared with the data from the horizontal displacement sensors in Dh6 and Dh3 (Figure 5-3). These have measured the elongation of the sensors installed in three directions in each deposition hole between the rock wall and canister top in Dh6 (canister bottom in Dh3), and have displayed maximum values (11 and 6 mm, respectively) which were fairly similar to the results for the wet case model.

It can be noted that the displacement in both model cases decreased during the latter phase of the process and equilibrated at a final value of approximately 3-4 mm. This reflects the overall homogenisation, caused by the saturation process, and a small remaining heterogeneity which is caused by the hysteretic behaviour of the used model.

Figure 5-1. Results from 2D_dry model. Dry density after 8 and 21 years (upper). Displacement evolution with maximum after 10-15 years (lower).

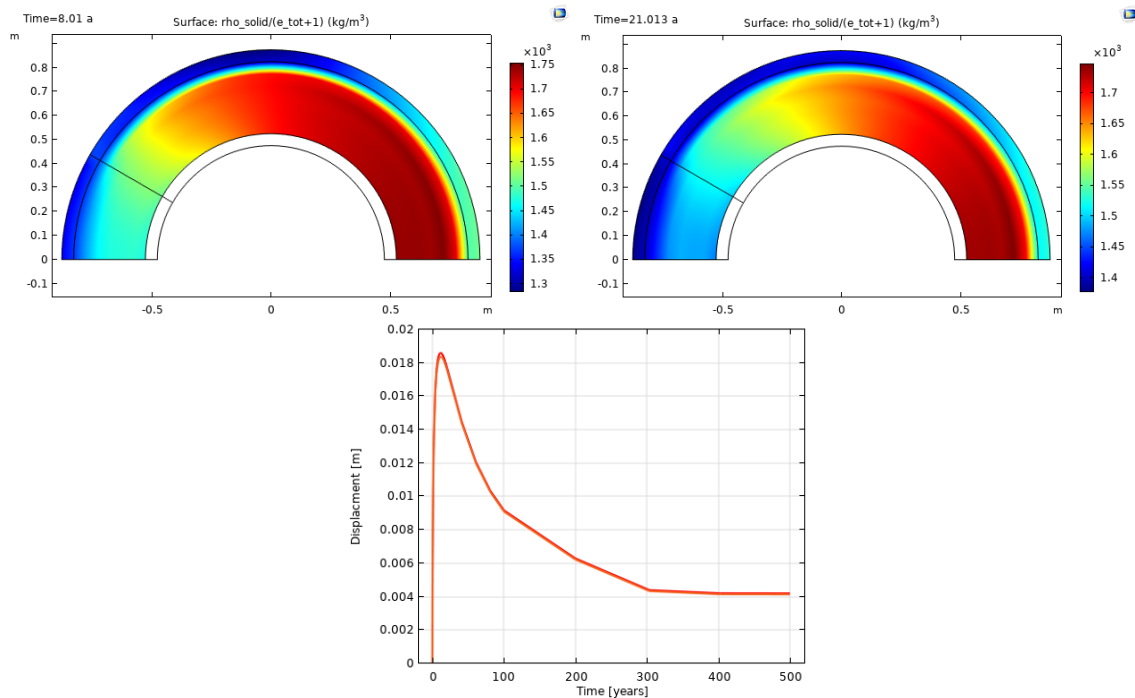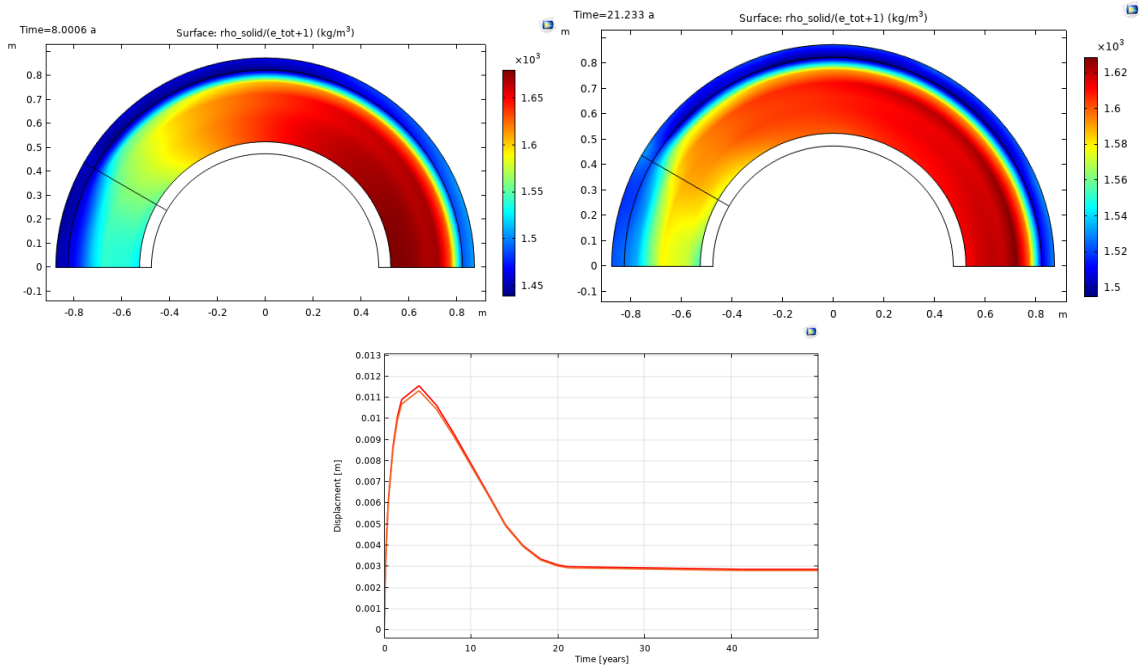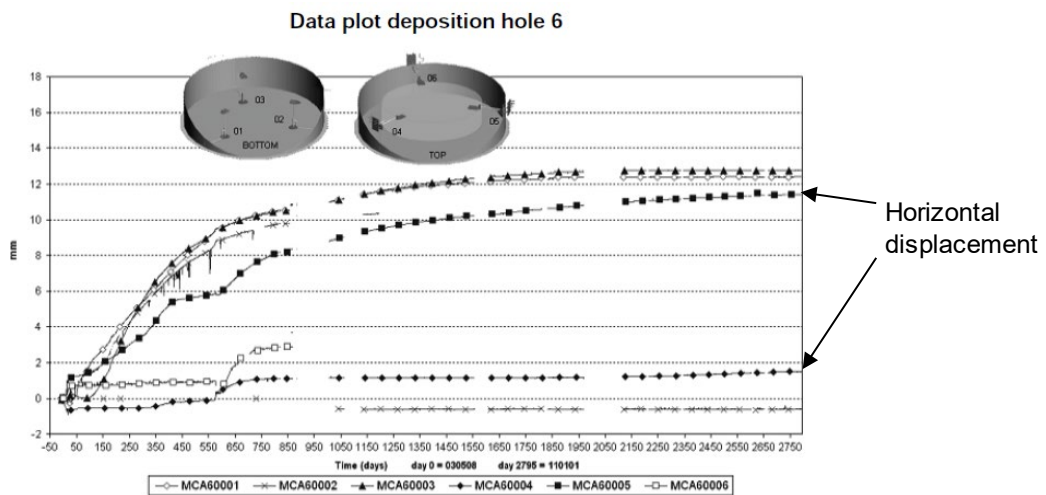*Figure 5-2. Results from 2D_wet model. Dry density after 8 and 21 years (upper). Displacement evolution with maximum after 4 years (lower).*

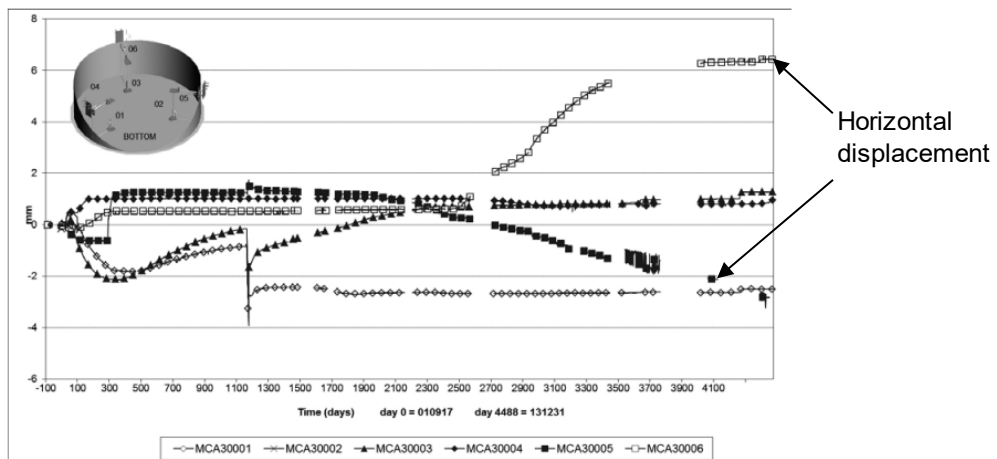## A5.4 Data plot deposition hole 3

Figure 5-3. Measured displacements in Dh6 and Dh3 (from Svemar et al. 2016 and Goudarzi 2015).

6 Prediction of direction of highest dry density in Dh3

Based on the data from the sensors for measurements of horizontal displacements in Dh3, it can be predicted in which direction the highest dry densities of the buffer will be found. The last registered results from sensor MCA30006 and MCA30005 was +6.5 and -2.0 mm, respectively (see Figure 5-3). The signal from MCA30004 had indicated an almost constant displacement of approximately +1 mm throughout the entire measuring period. Due to this, and the fact that this displacement was incompatible with the results from the other two sensors, it was disregarded. Together with the orientation of the different sensors (see Barcena and Garcia-Sineriz 2001) it can be anticipated that the direction of the resultant displacement has an orientation of little more than 190°, i.e. approximately towards east (Figure 6-1).

This approach can also be applied for the canister in Dh6, for which the most distinctive horizontal displacement of approximately 11 mm was registered by the MCA6005-sensor (see Figure 5-3). This sensor was installed in Ring 10 and attached to the upper lid of the canister in the same direction as for MCA3005 in Dh3 (Goudarzi and Johannesson 2010), i.e. in direction 265°. This correlates quite well with the direction in which the lowest dry density values and the highest water contents were found in the upper rings of Dh6 (see Figure 2-2). This correlation seems however to be at odds with evaluation presented by Svemar et al. (2016), according to which the registered displacement of 11 mm was "judged to be an artifact".
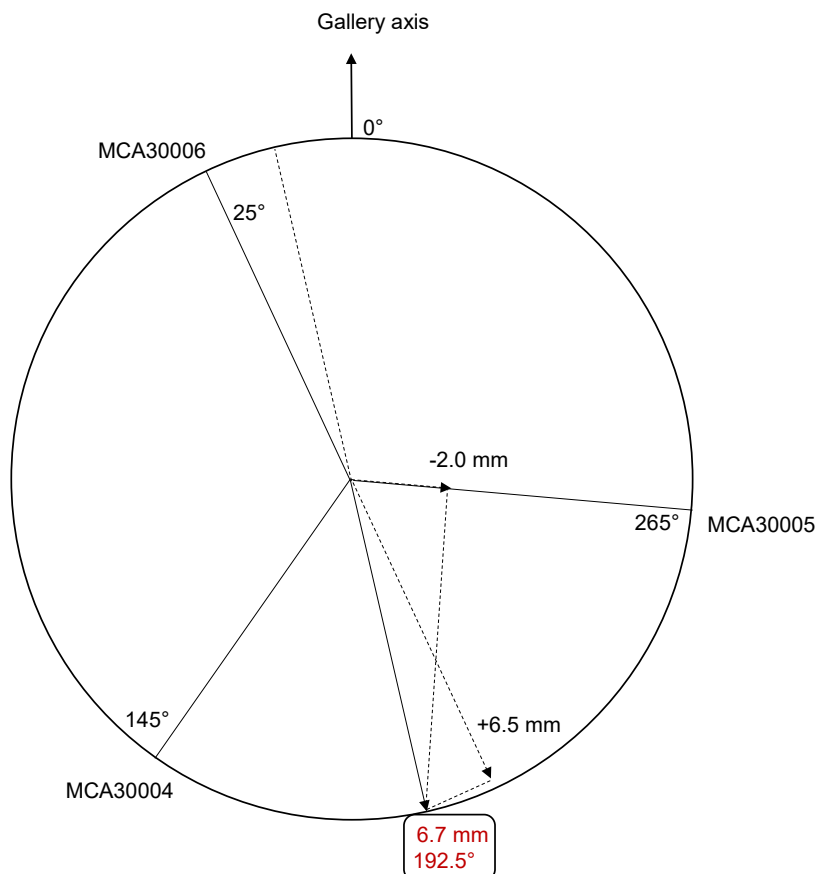

Figure 6-1. Tentative evaluation of last results from horizontal displacements sensors in Dh3. Resultant displacements vector marked red.

7 Final remarks

The following remarks can be made regarding buffer homogenisation and the planning of the dismantling and sampling of the inner section of the Prototype Repository:

i. It is important to perform a detailed analysis of the outer end sectors. These are the parts of the buffer which may yield the most important information regarding the homogenisation process. Nevertheless, the inner end sectors and the drill cores are also of great importance.

ii. The presented 1D models have predicted that the largest heterogeneity in terms of the dry density difference across the block-pellets interface is found for the case with a slow hydration and without a thermal gradient. Test conditions which resembles this case could possibly be found in dry parts of Dh2, in which the heater failed after ~3 years.

iii. If the displacement sensors MCA3006 and MCA3005 in Dh3 have displayed accurate results, then it should be possible to predict in which direction the highest dry densities will be found.

iv. There are thus motives for performing detailed analyses of all four depositions holes; Dh4: lowest inflow rate; Dh1: highest inflow rate; Dh2: lowest thermal gradient; and Dh3: potential prediction of direction with the highest dry density.

v. If the 2D model results are representative for the conditions in the inner section, then it can be expected that the dry density distribution will be less heterogenous than in the outer section.

The following remarks can be made regarding buffer homogenisation and the used material model:

i. The presented models demonstrate that the used material model can predict the homogenisation process for different boundary conditions in a consistent manner.

ii. If it however is found that the dry density difference across the block-pellets interface decreases with time, then this would indicate that hysteretic effects of the bentonite also decreases with time. Such a finding may therefore motivate the introduction of time-dependences in the material model.

iii. During the course of the work with the 2D geometry in this task, it was found that it was not possibly to reach convergence if the mesh of pellets-filled slot included more than one element in radial direction. This may reflect a shortcoming of the current formation of the material (i.e. the derivative of the path variable), which therefore should be further refined.

References

SKB's (Svensk Kärnbränslehantering AB) publications can be found at www.skb.com/publications.

Barcena I, Garcia-Sineriz J-L, 2001. Äspö Hard Rock Laboratory. Prototype Repository. System for canister displacement tracking. SKB IPR-02-06, Svensk Kärnbränslehantering AB.

Börgesson L, Gunnarsson D, Johannesson L-E, Sandén T, 2002. Äspö Hard Rock Laboratory. Prototype Repository. Installation of buffer, canisters, backfill and instruments in Section 1. SKB IPR-02-23, Svensk Kärnbränslehantering AB.

Börgesson L, Johannesson L-E, Sandén T, Hernelind J, 1995. Modelling of the physical behaviour of water saturated clay barriers. Laboratory tests, material models and finite element application. SKB TR 95-20, Svensk Kärnbränslehantering AB.

Börgesson L, Åkesson M, Hernelind J, 2020. EBS TF – THM modelling. Homogenisation task. SKB P-18-05, Svensk Kärnbränslehantering AB.

Charlier R, Darde B, Talandier J, Scaringi G, Mašín D, Poskas P, Narkuniene A, Justinavicius D, Kristensson O, Malmberg D, Newson R K, Thatcher K E, Zdravkovic L, Pedone G, Potts D, Tsiampousi A, Bosch J A, Ferrari A, Laloui L, Beese S s, Kumar V, Gramegna L, Villar M V, 2021. Specifications for beacon WP5: testing, verification and validation of models. Step 3-predictive test cases. Deliverable D5.6 Report, BEACON.

Dueck A, Börgesson L, Kristensson O, Malmberg D, Åkesson M, Hernelind J, 2019. Bentonite homogenisation. Laboratory study, model development and modelling of homogenisation processes. SKB TR-19-11, Svensk Kärnbränslehantering AB.

Dueck A, Nilsson U, 2010. Thermo-hydro-mechanical properties of MX-80. Results from advanced laboratory tests. SKB TR-10-55, Svensk Kärnbränslehantering AB.

Goudarzi R, 2014. Prototype Repository – Sensor data report (Period 010917–130101). Report No 25. SKB P-13-39, Svensk Kärnbränslehantering AB.

Goudarzi R, 2015. Prototype Repository – Sensor data report (Period 010917–140101). Report No 26. SKB P-14-30, Svensk Kärnbränslehantering AB.

Goudarzi R, Johannesson L-E 2010. Äspö Hard Rock Laboratory. Sensor data report No 23. SKB IPR-10-18, Svensk Kärnbränslehantering AB.

Johannesson L-E, 2014. Prototype Repository. Measurements of water content and density of the excavated buffer material form deposition hole 5 and 6 and the backfill in the outer section of the Prototype Repository. SKB P-13-14, Svensk Kärnbränslehantering AB.

Karnland O, Olsson S, Nilsson U, 2006. Mineralogy and sealing properties of various bentonites and smectite-rich clay material. SKB TR-06-30, Svensk Kärnbränslehantering AB.

Karnland O, Nilsson U, Weber H, Wersin P, 2008. Sealing ability of Wyoming bentonite pelletsforeseen as buffer material – Laboratory results. Physics and Chemistry of the Earth 33, 472–475.

Olsson S, Jensen V, Johannesson L-E, Hansen E, Karnland O, Kumpulainen S, Kiviranta L, Svensson D, Hansen S, Lindén J, 2013. Prototype Repository. Hydro-mechanical, chemical and mineralogical characterization of the buffer and tunnel backfill material from the outer section of the Prototype Repository. SKB TR-13-21, Svensk Kärnbränslehantering AB.

Svemar C, Johannesson L-E, Grahm P, Svensson D, Kristensson O, Lönnqvist M, Nilsson U, 2016. Prototype Repository. Opening and retrieval of outer section of Prototype Repository at Äspö Hard Rock Laboratory. Summary report. SKB TR-13-22, Svensk Kärnbränslehantering AB.

Åkesson M, Börgesson L, Kristensson O, 2010. SR-Site Data report. THM-modelling of buffer, backfill and other system components. SKB TR-10-44, Svensk Kärnbränslehantering AB.

Appendix A. Constitutive relations

HBM model

The HBM model is built around a number of defined equations and functions. The most important of these is a thermodynamic relation for the chemical potential of the clay water at water saturated conditions, which essentially states that the sum of the pressure (p) and suction(s) is equal to a quantity, denoted the clay potential (Ψ), which in turn is strongly related with the water content (w). If the clay is confined and has free access of water (s=0), then this means that the clay potential is equal to the swelling pressure. Correspondingly, if the clay can swell freely (p=0), then this means that the clay potential is equal to the suction. This can be expressed in tensor notation as:

$$sI - \frac{\sigma}{\alpha} = \Psi \qquad \qquad \text{A-1}$$

where the stress tensor (σ), the unit tensor (I) and also the clay potential (Ψ) are second order tensors. It can be noted that the stress is divided with a quantity, denoted the contact area fraction (α), which represents the ratio between the contact area between water saturated grains and the total area (Figure A-2, left). The value of this is 1 at water saturated conditions, and between 0 and 1 at unsaturated conditions.

A second important relation defines how the clay potential varies with the water content. As a measure of the volumetric content the micro void ratio (e_μ) is defined as the ratio between the water-filled pore volume and the solid volume and equals $w \cdot \rho_s/\rho_w$, where ρ_s and ρ_w denote the solid density and the water density, respectively. The void ratio (e) is calculated as ρ_s/ρ_d-1, where ρ_d is the dry density ($e_\mu = e$, at water saturated conditions). The clay potential is generally a strictly decreasing function of the micro void ratio, but displays an interval which can be described as $\Psi_M \pm \Psi_{\Delta/2}$, where "the mid-line" ($\Psi_M$) and "the half allowed span" ($\Psi_{\Delta/2}$) both are scalars and functions of the micro void ratio (Figure A-1, left)

The actual state within this interval is specified with the "path variable" (f), which approximately can assign values between -1 and +1. This is the case for the principal directions of stresses. With a more general definition, also f is a second order tensor:

$$\Psi(e_\mu, f) = \Psi_M(e_\mu)I + \Psi_{\Delta/2}(e_\mu)f \qquad \qquad \text{A-2}$$

In general, the path variable increases during consolidation and dehydration, while it decreases during swelling and water uptake (Figure A-2, right), and if the material undergoes a strain (ε) in some direction, then this will influence the path variable and the clay potential in the same direction. The hysteretic properties of the material can be incorporated in the model in this way. Another property, which is important to include in the model, is that the largest difference between the path variable in different directions should not exceed 1. This means that the shear strength of the material can be described with the same mathematical expression as for the hysteresis. This is formulated in the following way:

$$\frac{\partial f_{\alpha\beta}}{\partial \varepsilon_{\alpha\beta}} = -K_{\alpha\beta} \begin{cases} f_{\alpha\beta}^{+} - f_{\alpha\beta} & \text{for } \dot{\varepsilon}_{\alpha\beta} < 0 \\ f_{\alpha\beta} - f_{\alpha\beta}^{-} & \text{for } \dot{\varepsilon}_{\alpha\beta} > 0 \end{cases} \qquad \qquad \text{A-3}$$

where $f_{\alpha\beta}^{+}$ and $f_{\alpha\beta}^{-}$ are two limiting values for the path variable in direction αβ, and where $K_{\alpha\beta}$ is a parameter which influences the slope for stress paths in the $e\mu$-Ψ plane.

The limiting values for direction αβ are calculated from the half-circle $f_q^2 + f_p^2 = R^2$, where f_q and f_p are defined in the same way as the von Mises stress and the mean stress are defined from the stress tensor, and under the condition that f in all other directions is constant (Figure A-2, right).
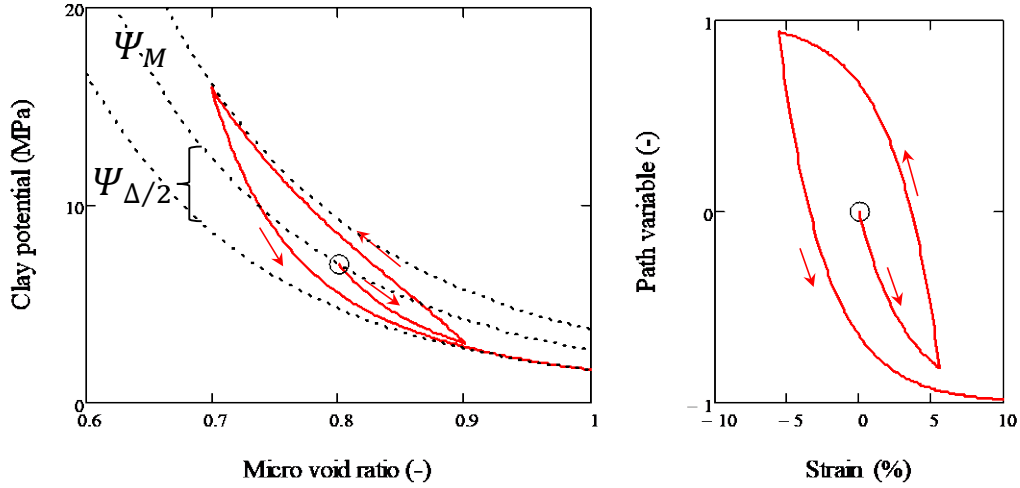
Figure A-1. Clay potential vs micro void ratio and path variable vs strain. Right panel shows an example with swelling, subsequent consolidation and final swelling. Left panel shows the same stress path mapped on the region for the clay potential.
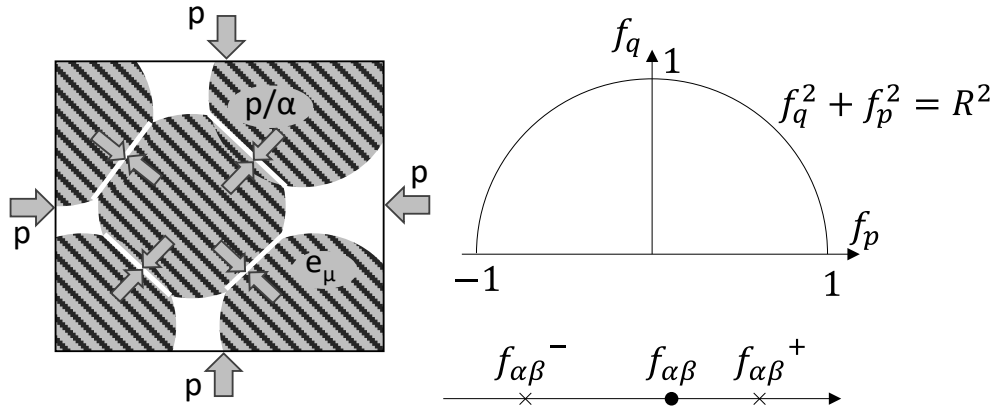

Figure A-2. Schematic illustration of a dual porosity with water-filled micro pores and gas-filled meso pores, and the distinction between overall pressure and contact pressure (left). Half- circle in f_q-f_p plane from which limiting values for individual path variables are calculated (right).

The density of water is defined as a function of the suction value:

$$\rho_w(s) = \rho_{w0} \exp(-\beta s)$$

A-4

where β is the compressibility of water and ρ_{w0} is a reference value. Equations A-1 to A-4 defines the HBM model for water saturated systems (when $\alpha = 1$).

In order to generalize the model for water unsaturated conditions, the contact area fraction (α) is defined as a function of the micro void ratio and the void ratio:

$$\alpha(e_\mu, e) = \left(\frac{1 + e_\mu}{1 + e}\right)^\gamma$$

A-5

where γ is a parameter.

Finally, one additional relation is required in order to define the system completely so that all variables can be calculated. Such a relation is defined as a differential with the two partial derivatives $\partial e_\mu/\partial e$ and $\partial e_\mu/\partial s$:

$$de_\mu = \frac{\partial e_\mu}{\partial e} de + \frac{\partial e_\mu}{\partial s} ds \qquad\qquad \text{A-6}$$

$$\frac{\partial e_\mu}{\partial e} = \alpha(e_\mu, e)^\eta$$

$$\frac{\partial e_\mu}{\partial s} = \begin{cases} \dfrac{(e - e_\mu)\Psi_M(e_\mu)}{s} \dfrac{1}{(e - e_\mu)\dfrac{\partial \Psi_M}{\partial e_\mu} - \Psi_M(e_\mu)} & \text{if } \dot{s} < 0 \\[2em] \dfrac{-e_{step}}{|s - \Psi_M(e_\mu - e_{step})|} & \text{otherwise} \end{cases}$$

The first derivative ($\partial e_\mu/\partial e$) should assume the value of 1 at water saturated conditions and lower values for unsaturated. The derivative is therefore assumed to be similar to α, but the parameter η is introduced in order to enable modifications of the derivative.

The second derivative ($\partial e_\mu/\partial s$) should be path dependent and two expressions have therefore been derived (Figure A-3). The first is used for decreasing suction values, and assumes that the ratio between suction and Ψ_M decreases linearly for increasing $e\mu$ towards the target point s=0 and $e_\mu=e$. The second expression for increasing suction implies that suction increases asymptotically towards the Ψ_M-line when e_μ decreases.

Parameter values for the HBM-model

The clay potential functions for MX-80 were adopted on the following form (Figure A-4):

$$\Psi_M(e_\mu) = \exp[m_0 + m_1 \cdot \text{erf}(e_\mu - 0.7) + m_2 \cdot e_\mu + m_3 \cdot e_\mu^{-0.5}] \qquad \text{A-7}$$

$$\Psi_{\Delta 2}(e_\mu) = \exp[d_0 + d_1 \cdot \text{erf}(e_\mu - 0.7) + d_2 \cdot e_\mu]$$

With the parameter values m_0=3.0591, m_1=-3.6389, m_2=-0.8276 and m_3=0.0443, and d_0=1.706, d_1=-3.5199 and d_2=-0.4838 for clay potential functions with the unit MPa. In addition to these functions, the following parameter values were used: K=40, γ=7, η=1, R=0.9 and e_{step}=0.01.
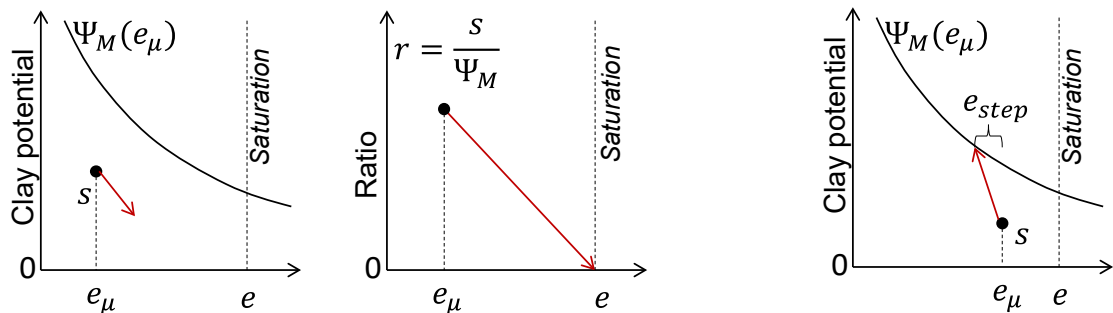

Figure A-3. Definition of $\partial e_\mu/\partial s$-derivative for decreasing suction (left) and increasing suction (right).
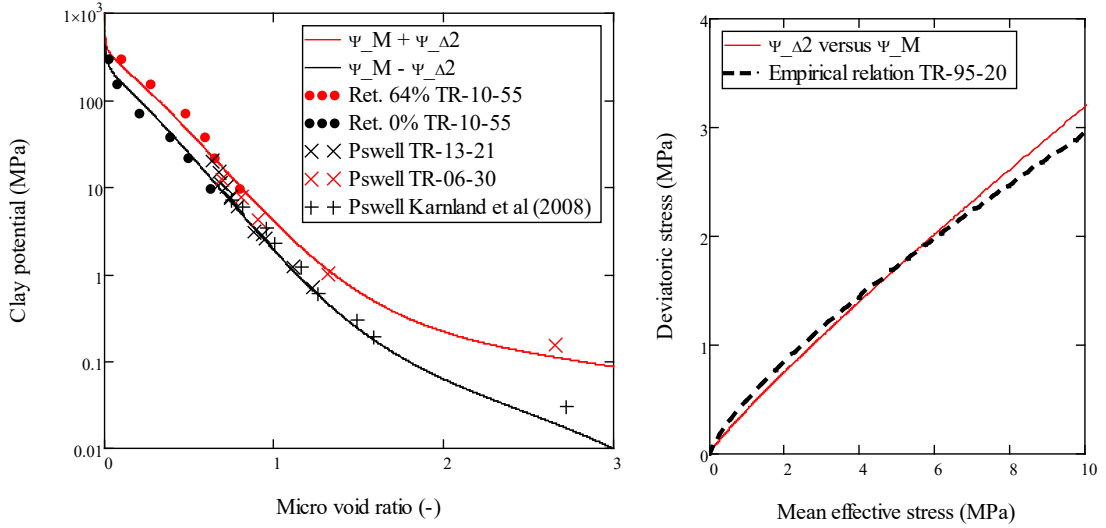
Figure A-4. Adopted clay potential functions. Comparison of clay potential function with retention and swelling pressure data (left), and with shear strength data (right). Experimental data marked for comparison: TR-13-21 and TR-06-30 are swelling pressure data for MX-80 from Olsson et al. (2013) and Karnland et al. (2006), respectively; data points marked Karnland et al. (2008) are also swelling pressures for MX-80; TR-10-55 is water retention data for samples with different initial water content (0 and 64 %) at free swelling conditions from Dueck and Nilsson (2010) for which the relative humidity was converted to a pressure (see Dueck at al. 2019) and the water content converted to a dry density at saturated conditions. The line in the right graph marked TR-95-20 is an empirical relationship between the maximum deviatoric stress versus the mean effective stress adopted from different triaxial compression tests by Börgesson et al. (1995).

Hydraulic transport model

Two water transport processes are included in the model. The first process is advective transport, described by Darcy´s law for unsaturated conditions. For this the permeability for MX-80 follows the parameter value adoption given by Åkesson et al. (2010):

$$k(e, e_\mu) = 2.4 \cdot 10^{-20} \cdot e^{-5.33} \cdot \left(\frac{e_\mu}{e}\right)^3 \quad (m^2) \qquad \text{A-8}$$

The second process is diffusion of water vapor, which like the Code_Bright implementation is driven by gradients in the mass fraction of vapor. The diffusion coefficient for this is calculated as:

$$D(e, e_\mu) = n \cdot \left(1 - \frac{e_\mu}{e}\right) \cdot \tau \cdot D_0 \cdot \frac{T^{2.3}}{p_g} \quad \left(\frac{m^2}{s}\right) \qquad \text{A-9}$$

where the tortuosity was set to τ =0.8, and the diffusion coefficient was set to D_0=5.9e-6 $m^2PaK^{-2.3}s^{-1}$ (Åkesson et al. 2010).

Thermal transport model

For simplicity, one thermal conductivity relation, which were adopted from the experimental data presented by Åkesson et al. (2010), were used for both the bentonite blocks and the pellets filling:

$$\lambda(e, e_\mu) = 0.5 \cdot \left(1 - \frac{e_\mu}{e}\right) + 1.3 \cdot \left(\frac{e_\mu}{e}\right) \quad \left(\frac{W}{m^2K}\right) \qquad \text{A-10}$$